Influence of Radiative Heat Transfer on Convective Flows in Aircraft Cabins

Lambert, Markus[1], Kessler, Roland[1], Rütten, Markus[2] and Wagner, Claus[2]

[1]German Aerospace Center (DLR), Institute of Aerodynamics and Flow Technology

$C^2A^2S^2E$ - Center for Computer Applications in Aero Space Science and Engineering

[2]German Aerospace Center (DLR), Institute of Aerodynamics and Flow Technology

FS - Fluid Systems

Bunsenstraße 10, 37073 Göttingen, Germany

Abstract

In this paper the influence of radiative heat transfer on convective flows in aircraft cabins is considered. The results show that in thermally driven flows radiation heat transfer have an essential impact on the flow and must be considered for accurate flow predictions. A parallel Discrete Transfer Radiation Method (DTRM) for the simulation of the surface to surface radiation heat transfer is coupled with the DLR THETA code. Besides the standard boundary condition for wall heat radiation, a special treatment for transparent boundaries is implemented. It offers the possibility to specify the radiation heat flux and the direction of incidence of the sun through the cabin window. The energy is then distributed in the cabin by the DTRM. The DLR THETA code is an unstructured incompressible Navier-Stokes-Solver developed by the German Aerospace Center (DLR). It supports convective heat transport, very large grids, highly complex geometries and massive parallel computations.

1 Introduction

The aircraft industry has to meet big challenges in the near future. Besides the need of a drastic reduction of noise and pollutants, the well-being of passengers comes more and more to the fore. The comfort of passengers is strongly influenced by the temperature and air velocity distribution inside the cabin. Numerical simulations of the cabin air flow will play an essential role in the design procedure and will help to reduce time-consuming experiments.

In many cases the air flow in the cabin is unsteady. This challenges the simulation software as well as the computer hardware. Further, due to the complexity of the geometry a large number of grid points have to be used for reliable flow predictions and the unsteadiness of the flow requires real simulation times of several minutes. The use of efficient numerical methods, which are well suited for modern, massively parallel computer systems, is therefore mandatory.

The simulations were done with the DLR THETA code, a finite volume code [9] which uses unstructured, hybrid grids. The code is based on data structures and libraries of the DLR TAU code [5]. However, the solution algorithms are optimized for the efficient simulation of incompressible flows. The variation of the density with respect to temperature differences is realized using the Boussinesq approximation [2] or the ideal gas law [3]. The implicit time-stepping allows stable solutions for large time steps. It provides inter alia the well known pressure correction projection method [6], [4], [16] for velocity pressure coupling. Applying a matrix-free formulation of conjugate gradient solvers [10] combined with a multi grid method [7], [17] provides an efficient linear equation solver. Domain decomposition is used in the DLR THETA code in order to get affordable CPU times on massively parallel computer systems for large scale problems.

As mentioned before radiative heat transfer is an essential phenomena in thermally driven flows. Due to the unsteadiness of cabin air flows it is necessary to couple the radiation module with the flow solver at each time-step. This dictates that memory and CPU-

time requirements for the radiation solver should ideally not exceed that of the Navier-Stokes-Solver itself. Additionally, the radiation module must be included in the parallelization concept of the Navier-Stokes-Solver.

We chose the Discrete Transfer Radiation Method (DTRM) for the simulation of the surface to surface radiation heat transfer including the incident solar heat through the cabin window. It shares similarities with the well known Radiation Simulation Monte Carlo Method [20], based on the transfer of independent radiative energy particles. These particles are emitted from each surface point in the computational domain but use only a finite number of fixed directions. In a preprocessing step the boundary surfaces of the computational grid which are located in these directions are identified and stored. During the simulation we directly transfer the radiative energy from surface to surface without tracing the trajectory of the energy particles. Since the DLR THETA code uses a domain decomposition approach for parallel computations, we decompose the stored surfaces such that each processor has a list of all boundary surfaces which can be reached from a boundary surface of its own domain. During the simulation we compute the DTRM step locally on each processor and then exchange all data in one communication step to avoid performance reduction due to communication. We restrict the number of discrete directions we choose for the DTRM due to memory limitations. In order to reduce statistical errors, a smoothing algorithm is used for the radiative energy distribution on the boundary surface. This method leads to accurate and smooth heat flux distributions even for a small number of discrete directions. In the above mentioned preprocessing we use an efficient ray-tracer algorithm [18], which is based on an element-to-element list thus avoiding element searches.

2 The Governing Equations and the Numerical Methods

2.1 The Reynolds-averaged Navier-Stokes-equations

We consider the Reynolds-averaged (RANS) formulation of the time-dependent, incompressible ($\rho \neq \rho(p)$)

Navier-Stokes-equations in a bounded domain $\Omega \in \mathbb{R}^3$ and in a time interval $(0, \tau)$

$$
\begin{aligned}
\frac{\partial (\rho \mathbf{v})}{\partial t} + \nabla \cdot (\rho \mathbf{v} \otimes \mathbf{v}) & \\
- \nabla \cdot (2 (\mu + \mu_\mathrm{t}) \, \mathbb{S} (\mathbf{v})) + \frac{2}{3} \rho k \mathbb{I} + \nabla p & = \rho \mathbf{f} \\
\frac{\partial \rho}{\partial t} + \nabla \cdot \rho \mathbf{v} & = 0.
\end{aligned}
$$

Here $\mathbf{v}$ denotes the velocity, p the pressure, ρ the density, $\mathbf{f}$ the force density of external forces like gravity, $\mu > 0$ the physical viscosity, $\mu_\mathrm{t} > 0$ the turbulent viscosity and k the turbulent kinetic energy. $\mathbb{S} (\mathbf{v}) = \frac{1}{2} \left(\nabla \mathbf{v} + \nabla \mathbf{v}^T \right)$ is the symmetric deformation velocity tensor and $\mathbb{I}$ the unit matrix. Additional boundary and initial conditions have to be formulated. Within this framework different turbulence models are available. The standard k-ω [19], Menters k-ω-SST [11] and SAS-SST [13], [12] turbulence models with universal wall functions [8] as well as the standard and modified k-ε [19] turbulence models are implemented. Also the standard buoyancy turbulence modification [15] is provided.

To simulate the influence of thermal convection, the temperature transport equation is solved

$$
\frac{\partial (\rho T)}{\partial t} + \nabla \cdot (\rho T \mathbf{v}) = \nabla \cdot \left(\left(\frac{\kappa}{c_\mathrm{p}} + \frac{\mu_\mathrm{t}}{Pr_\mathrm{t}} \right) \nabla T \right) \quad (1)
$$

for the temperature T. In this equation c_p denotes the specific heat capacity, κ the thermal conductivity and Pr_t the turbulent Prandtl number. Appropriate boundary conditions, e.g. a von Neumann boundary condition at walls

$$
\mathbf{n} \cdot \left(\left(\frac{\kappa}{c_\mathrm{p}} + \frac{\mu_\mathrm{t}}{Pr_\mathrm{t}} \right) \nabla T \right) = \frac{\|\mathbf{n}\|}{c_\mathrm{p}} \left(q_\mathrm{w} + q_\mathrm{rad} \right) \quad (2)
$$

with the boundary normal vector $\mathbf{n}$, a wall heat flux q_w and the radiation heat flux q_rad are implemented. The radiation heat flux q_rad caused by surface to surface heat radiation is computed by the DTRM. The wall flux q_w is set fixed or calculated by $q_\mathrm{w} = (T_\mathrm{w} - T) \alpha_\mathrm{w}$ with a fixed outer wall temperature T_w and the heat transfer coefficient α_w of the wall material. Variable density due to buoyancy is modeled using the Boussinesq approximation [2] $\rho = \rho(T) = \rho_\infty (1 - \beta(T - T_\infty))$ with the reference Temperature T_∞, the reference density ρ_∞ and the

thermal expansion coefficient β or the ideal gas law [3] $\rho = \rho(T) = \frac{p_\infty}{R_G T}$ with the reference pressure p_∞ and the gas constant $R_G = 287 \frac{J}{KgK}$ of air.

2.2 Surface Heat Radiation

Any surface at a temperature above 0 K radiates energy. The amount of energy E (per unit surface area and unit time) a solid surface of a so called Gray Lambert radiator emits is given by the Stefan-Boltzmann law

$$E(T) = \varepsilon(T)\sigma T^4, \; \sigma = 5,67051 \cdot 10^{-8} \frac{W}{m^2 K^4}. \quad (3)$$

Here σ is the Stefan-Boltzmann constant and

$$\varepsilon(T) = \frac{1}{\sigma T^4} \int_0^\infty \int_0^{2\pi} \int_0^{\frac{\pi}{2}} \varepsilon_\lambda^{\mathrm{d}}(\theta, \phi, \lambda, T) I_{b,\lambda}(\lambda, T) \\ \cos(\theta)\sin(\theta)\, d\theta\, d\phi\, d\lambda$$

is the emissivity. It is defined by integration over all directions θ, ϕ and all wavelengths λ of the so called directional spectral emissivity $\varepsilon_\lambda^{\mathrm{d}}(\theta, \phi, \lambda, T) = \frac{I_\lambda(\theta,\phi,\lambda,T)}{I_{b,\lambda}(\lambda,T)}$. The directional spectral emissivity describes the ratio of the emissive radiation intensity I_λ of some body and the emissive radiation intensity $I_{b,\lambda}$ of a black body, which have the same temperature. The emissive power emitted uniformly in all directions from an infinitesimal area dA into a solid angle $d\Omega$ is described by Lambert's cosine law

$$dq = I_\lambda(\theta, \phi, \lambda, T)\cos(\theta)\, dA\, d\Omega, \; d\Omega = \sin(\theta)\, d\theta\, d\phi. \quad (4)$$

The proportionality factor $I_\lambda(\theta, \phi, \lambda, T)$ is the directional spectral intensity of radiation. A more detailed description of the radiation heat transfer physics can be found in [1].

For each wall surface F of the computational grid we compute a fixed number of directions for the DTRM in the following way. First we choose equidistant distributed numbers $R^i = \frac{i}{n_\phi}, R^j = \frac{j}{n_\theta} \in (0,1), i = 0 \ldots n_\phi - 1, j = 1 \ldots n_\theta, \; n_\phi, n_\theta \in \mathbb{N}$. Let $\mathbf{n}_F$ be the surface normal and $\mathcal{R}_{\mathbf{n}_F}$ the rotation matrix, which rotates the vector $(1,0,0)^T$ into the direction of the surface normal, i.e. $\mathcal{R}_{\mathbf{n}_F}(1,0,0)^T = \frac{\mathbf{n}_F}{\|\mathbf{n}_F\|}$. Since the directional distribution must fulfill Lambert's cosine law (4), we set $\phi^i = 2\pi R^i, \theta^j = \arccos\left(\sqrt{1 - R^j}\right)$

and get in spherical coordinates $\mathbf{d}_F^{i,j} = \mathcal{R}_{\mathbf{n}_F} \mathbf{d}^{i,j}, \mathbf{d}^{i,j} = \left(\sin\theta^j \cos\phi^i, \sin\theta^j \sin\phi^i, \cos\theta^j\right)^T$, $d_F^{0,0} = \mathcal{R}_{\mathbf{n}_F}(1,0,0)^T = \frac{\mathbf{n}_F}{\|\mathbf{n}_F\|}$.

For each transparent boundary surface, i.e. a window boundary surface, we can specify the direction of incidence $\mathbf{d}_F^{inc}$ of the sun. In this case we set $\mathbf{d}_F^{i,j} = \mathbf{d}_F^{inc}, i = 0 \ldots n_\phi - 1, j = j = 0 \ldots n_\theta$ to get the same amount of directions as in the wall surface case.

Then we send rays in these directions and trace them through the computational domain. If they hit a boundary surface we store this surface index in a special surface list associated to the sending surface. For each radiative wall surface we have finally the above-named list of goal surfaces, which can be reached by a ray emitted by this surface. These lists are stored.

We consider each radiative wall surface F of the computational grid as a Gray Lambert radiator and send a fixed number N_P of energy-particles, which carry the uniformly distributed radiation heat energy given by (3), i.e. each particle transfers the energy $e_P = \frac{\varepsilon\sigma T_F^4 \|\mathbf{n}_F\|}{N_P}$. Randomly one of the surfaces from the list of goal surfaces is chosen and the energy of the particle is added to the received energy of this surface. Each transparent boundary surfaces F of the computational grid are treated similarly. We send the same fixed number N_P of energy-particles but with the energy $e_P = \frac{E_{sun}\|\mathbf{n}_F\|}{N_P}$ where E_{sun} is the radiation heat flux, i.e. the amount of energy per surface area due to the sun irradiated through the transparent boundary surface. Similar to the wall surface case, one of the surfaces from the list of goal surfaces is chosen randomly and the energy of the particle is added to the received energy of this surface. But in this case all the surfaces from the list of goal surfaces are identical because they are located in the same direction, namely the direction of incidence $\mathbf{d}_F^{inc}$. This allows to use the same data-structure in sun and wall radiation treatment.

Since each surface is a member of the goal surface list of several other surfaces we sum up all the received energy contributions of one DTRM step. Let E_F^0 denote this sum of received energy. Then εE_N^0 is absorbed by the surface and $(1 - \varepsilon)E_F^0$ is reflected. So finally a so called wall reflection iteration is

realized, i.e. a fixed number N_{iter} of additional surface heat radiation steps by DTRM with the energy $e_P^{n+1} = \frac{E_F^{n+1}}{N_P}, E_F^{n+1} = (1 - \varepsilon)E_F^n, 0 \leq n < N_{iter}$ are performed.

3 Results

We simulated the mixed convection flow in a generic wide-bodied aircraft cabin segment mock-up (figure 1) with six rows per eight seats, where thermal dummies are seated. Complex boundary conditions are realized taking into account the thermal influence of light-bands, different wall segments, seating benches, air condition inlets and outlets and sun heat radiation through plane cabin windows. We have two rows each with five air inlets which consists of two slots. They are located at the top of the cabin-floor over the corridors and marked light blue in figure 2. The outlets, seven per side-wall, are located close over the cabin-bottom. They are marked red in figure 2. All in all four light-bands, marked yellow in figure 2, are installed. Finally, we have one cabin-window per row and side, marked gray in figure 2. The front-side and the back-side of the mock-up were closed by walls.

The thermal boundary conditions, shown in figure 3, are specified according to the set-up of experiments done in a mock-up at the German Aerospace Center (DLR). The heat power emission of the dummies is modeled by a fixed heat flux over the their entire surface. The emission coefficients of the materials are taken from the literature. The inflow velocity profiles at the inlets correspond to those realized in the experiments, which were done for a inflow rate of $540\ l/s$. In this case an inflow temperature of $T_{inf} = 286.55K$ was measured and also specified in the simulation. We have chosen these settings since the boundary conditions, especial the inflow velocities strongly influence the flow. Therefore they have to be modeled accurately in order to allow comparisons with the measurements. We computed three different simulation scenarios, time-dependent thermal simulation with and without heat radiation, and time-dependent thermal simulation with heat radiation and additional sun heat radiation through the cabin windows. In the last simulation scenario the angle of incidence for the sun heat radiation was set to $30°$ and the incidence direction lay in the y-z-plane, i.e. the direction of incidence was set to

$\mathbf{d}_F^{inc} = (0,\ 1,\ 0.57735027)^T$. The radiation heat flux due to sun incidence was set to $400\frac{W}{m^2}$, which is a rough estimate calculated starting from the solar constant of $1367\frac{W}{m^2}$ taking into account the distance the sun radiation has to pass through the atmosphere and the flat angle of incidence as well as the absorption by the heat protection glass of nearly 50 to 70 percent.

All computations were done on the same hybrid unstructured grid with 4.3 million points. We simulated a physical time of $360s$. After a preliminary lead time of $120s$ the quantities of interest are time-averaged over $240s$. The numerical time step was fixed to $0.2s$. We did a parallel computation on 64 processors and chose the second order QUDS scheme in space and a second order scheme in time. The standard k-ω-turbulence-model [19] with universal wall functions [8] and a $V4$ multi-grid circle was used for solving the pressure correction equation. Variable density due to buoyancy was modeled using the Boussinesq approximation [2]. Due to the unsteadiness of the considered flow we coupled the radiation module with the flow solver each time-step. For the DTRM we used 257 fixed directions per wall boundary surface in the computational grid (16 for zenith angle times 16 for azimuth angle plus the surface normal direction). Per time step we made 100 DTRM steps and averaged the radiation heat flux over this 100 steps to reduce the statistical errors. In each DTRM step we sent 50 rays per surface and made five wall reflection iteration steps.

Figure 4 shows the computed differences in the surface temperature distribution of the model dummies with and without heat radiation. It is concluded that modeling the heat transport by surface to surface heat radiation leads to averaged temperature of the dummies surfaces which are significant lower. Changing the model dummy surface temperatures directly influences the flow in the cabin. If we consider the magnitude of the time averaged velocity in the two cut planes shown in figure 4 located at $x = 0.928$ and $x = -2.880$ it looks marginal at first sight. But if we consider the isoplanes of the magnitude of the time averaged velocity value 0.2 without modeling heat radiation as shown in figure 8 and with modeling heat radiation as shown in figure 9, a significant change in the flow field topology is observed. Figures 5 and 6 reflect the comparison between time averaged velocity magnitude in the simulation (with radiation heat transfer) and in the mea-

surements in two different planes. These planes are the experimental cut planes of the PIV (Particle Image Velocimetry) conducted in a mock-up at the German Aerospace Center (DLR). All main features of the flow observed in the experiments are reproduced by the numerical simulation. The quantitative differences can be ascribed to the high sensitivity of the unsteady flow even to small changes of the boundary conditions, as well as to a strong three dimensional character of the flow.

Additionally modeling the presence of incidence of the sun through the cabin windows, the flow field changes again significant as shown in figure 10. Figure 7 shows the surface temperature distribution of the model dummies in the sun heat radiation case. The surface temperature of dummy parts which are directly hit by the sun heat radiation like the head or neck is increased. The dummies sitting in front of the windows on the sun shadow side are cooled due to absence of heat radiation reflection at the full transparent cabin windows. Considering the surface temperature of the model dummies in detail as shown in figure 11 (left), one observes that the computed surface temperatures are about $330K \approx 57°C$. This is far away from temperatures which occurs in real human skin case [14]. The thermal model of the dummies we use in the simulations as well as in the experiments seems to be responsible for these effects. To investigate this real behavior of the model dummies we spotlighted one of them by a $1000W$ lamp from a distance of $1.89m$ and measured the surface temperature by a thermo camera. The results is shown in figure 11 (left). Due to technical reasons the lamp was spotlighting the dummy from the front side right so that the main focus was located on the breast and not on the head as in our simulation and the lamp had a big scattering angle so that the energy was not as focused as in the simulation. Due to this technical necessities we have chosen a higher power lamp to make sure that a power of approximate $400\frac{W}{m^2}$ reach the dummy surface. However we can see that almost $60°C$ is reached in the spotlight focus area at the breast of the dummy. We conclude that the implemented thermal boundary condition for the dummies surfaces are suitable to model real human persons in a aircraft cabin if the dummies are the only heat source. In this case the dummies are heated and emit about $80W$ heat power to the environment like a real human body. If additional heat sources, like sun heat radiation, came into play the fixed flux model is far away from reality. More complicated boundary conditions modeling the real human skin behavior have to be implemented. Also in the experimental set-up more complicated model dummies have to be used which supports a more realistic heat balancing.

4 Conclusions

A successful coupling of a DTRM with the DLR THETA Code was performed. The memory and CPU-time requirements of the radiation computations do not exceed those of the Navier-Stokes-Solver itself, even for a coupling at each time step. The radiation module is well parallelized and embedded in the parallelization concept of the DLR THETA code based on a domain decomposition approach.

We simulated the mixed convection flow in a generic wide-bodied aircraft cabin segment mock-up with six rows per eight seats. The seats are taken by model dummies. Complex boundary conditions are realized including the thermal influence of light-bands, different wall segments, seating benches, air condition inlets and outlets and air plane cabin windows with sun heat irradiation. The thermal boundary conditions are aligned to the set-up of the experiments done in a mock-up at the German Aerospace Center (DLR).

All main features of the flow, which are observed in the experiments, are reproduced by the numerical simulation but quantitative differences are observed. The reason might be the high sensitivity of the unsteady flow to the boundary conditions as well as the strong three dimensional character of the flow. To overcome this difficulties we have to reproduce the real experimental boundary conditions of the set-up of experiments more accurate in the simulation.

The results show a significant effect on the surface temperature for the various dummies if radiation heat transport is considered or the sun heat radiation trough the cabin windows is taken into account. Therefore in thermally driven indoor flows radiation heat transfer play an important role and must be considered for accurate flow predictions. The implemented thermal boundary condition for the dummies surfaces are suitable to model real human persons in a aircraft cabin if the dummies are the only significant heat source. If ad-

ditional heat sources like sun heat radiation came into play more complicated boundary conditions modeling the real human skin behavior have to be specified in the simulation and in the experimental set-up with respect to more complicated model dummies which supports a more realistic heat balancing.

References

[1] H. D. Baehr and K. Stephan. *Wärme- und Stoffübertragung*. Springer Verlag, Berlin, Heidelberg, New York, 2008.

[2] J. Boussinesq. *Théorie Analytique de la Chaleur*. Gauthier-Villars, Paris, 1903.

[3] C. Cercignani, R. Illner, and M. Pulvirenti. *The Mathematical Theory of Dilute Gases*. Springer Verlag, Berlin, Heidelberg, New York, 1994.

[4] A. J. Chorin. Numerical solution of the Navier-Stokes equations. *Math. Comp.*, 22:745–762, 1968.

[5] T. Gerhold, M. Galle, O. Friedrich, and J. Evans. Calculation of complex three-dimensional configurations employing the DLR TAU code. *AIAA Paper*, 97-0167, 1997.

[6] K. Goda. A multistep technique with implicit difference schemes for calculating two- or three-dimensional cavity flows. *J. Comput. Phys.*, 30:76–95, 1979.

[7] W. Hackbusch. *Multi-Grid Methods and Applications*. Springer Verlag, Berlin, Heidelberg, New York, 1985.

[8] T. Knopp. Model-consistent universal wall-functions for rans turbulence modelling. *Proceedings Intern. Conf. BAIL, Göttingen*, July 2006.

[9] D. Kröner. *Numerical Schemes for Conservation Laws*. Wiley and Teubner, 1997.

[10] A. Meister. *Numerik linearer Gleichungssysteme*. Vieweg, Braunschweig, Wiesbaden, 1999.

[11] F. R. Menter. Zonal two equation k- turbulence models for aerodynamic flows. *AIAA Paper*, 93-2906, 1993. AIAA 24th Fluid Dynamics Meeting, Orlando, July 1993.

[12] F. R. Menter. A scale-adaptive simulations model using two-equation models. *AIAA Paper*, 2005-1095, 2005. Reno.

[13] F. R. Menter and Y. Egorov. Re-visiting the turbulent scale equation. *Proc. IUTAM Symposium; One hundred years of boundary layer research, Göttingen*, 2004.

[14] H. Reuter. Zur Berechnung kurzfristiger Änderungen der menschlichen Hauttemperatur. *Theoretical and Applied Climatology*, 4(2):213–222, 1952.

[15] W. Rodi. *Turbulence models and their application in hydraulics - a state of the art review*. International Association for Hydraulic Research, Delft, 1993.

[16] L. J. P. Timmermans, P. D. Minev, and F. N. Van De Vosse. An approximate projection scheme for incompressible flow using spectral elements. *Int. J. Numer. Methods Fluids*, 22:673–688, 1996.

[17] U. Trottenberg, C. W. Oosterlee, and A. Schüller. *Multigrid*. Academic Press, London, 2001.

[18] M. Widhalm, A. Ronzheimer, and J. Meyer. Lagrangian particle tracking on large unstructured three-dimensional meshes. *American Institute of Aeronautics and Astronautics, 46th AIAA Aerospace Sciences Meeting and Exhibit [2008-01-07 - 2008-01-10], Reno, Nevada, U.S.A*, 2008. AIAA Reno 472.

[19] D. C. Wilcox. *Turbulence Modeling for CFD*. DCW Industries, Inc., 2006.

[20] W. J. Yang, H. Taniguchi, and K. Kudo. *Radiative Heat Transfer by the Monte Carlo Method*, volume 27 of *Advances in Heat Transfer*. Academic Press, 1995.
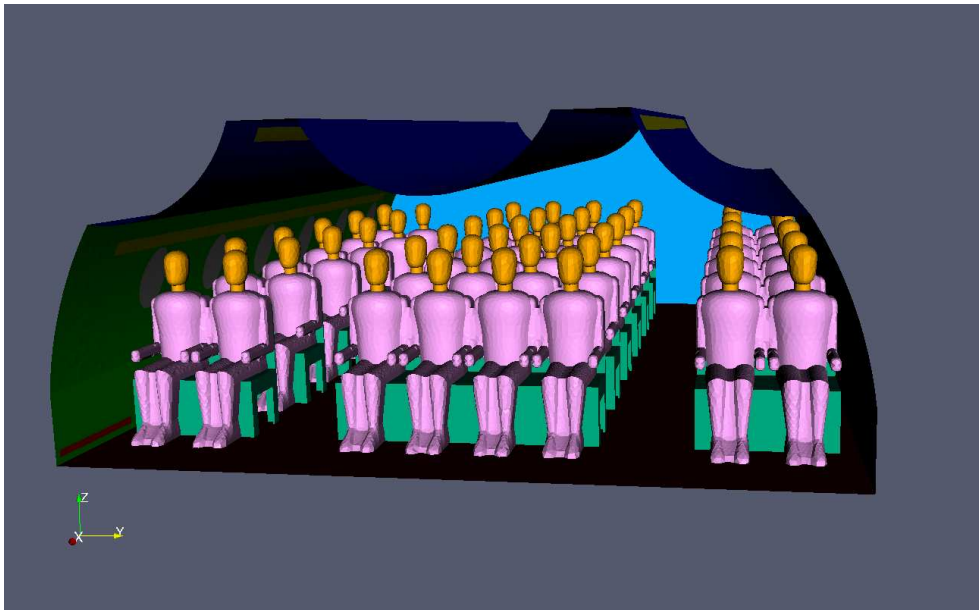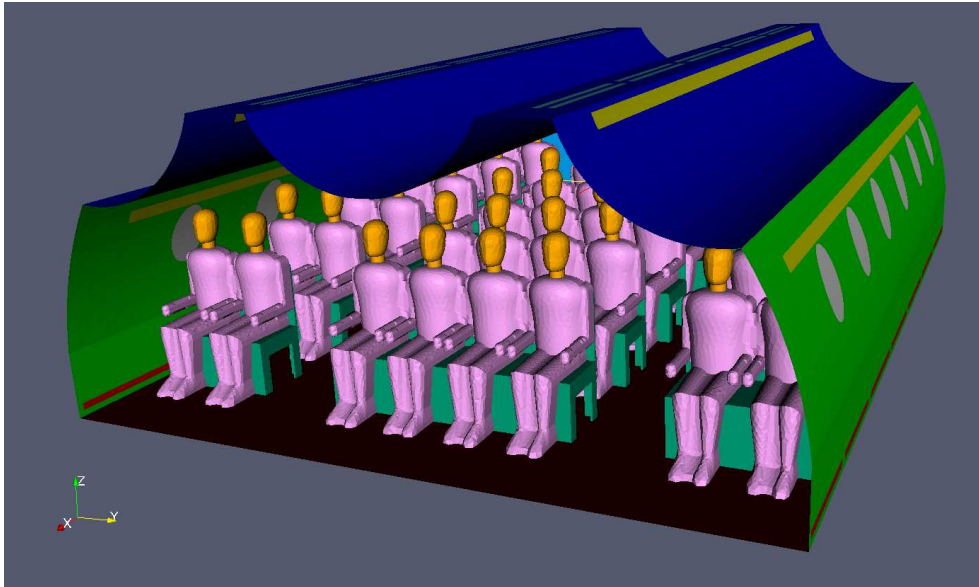
Figure 1. Geometry, generic wide-bodied aircraft cabin segment mock-up with six rows per eight seats and one window per side and row. The seats are taken by model dummies.
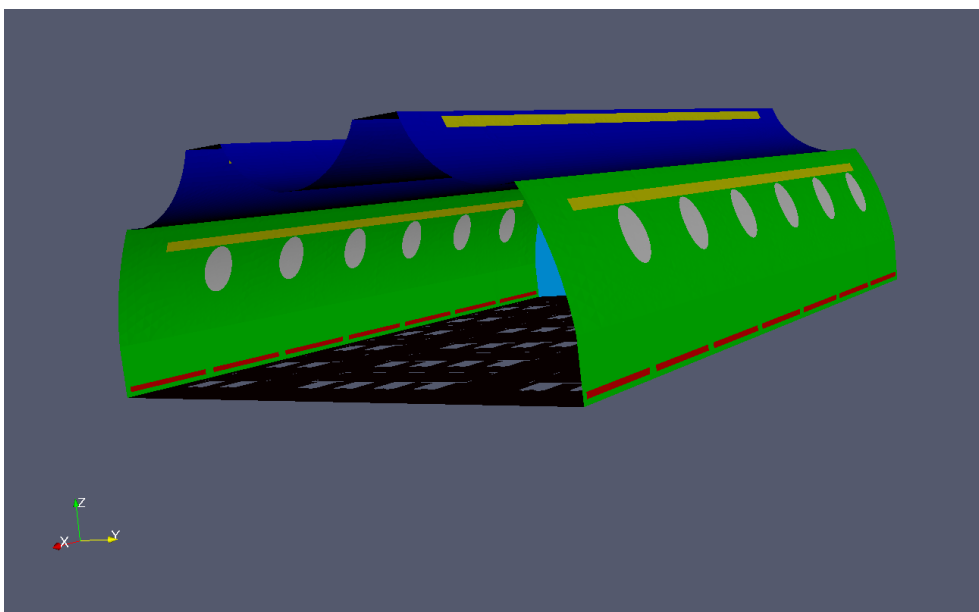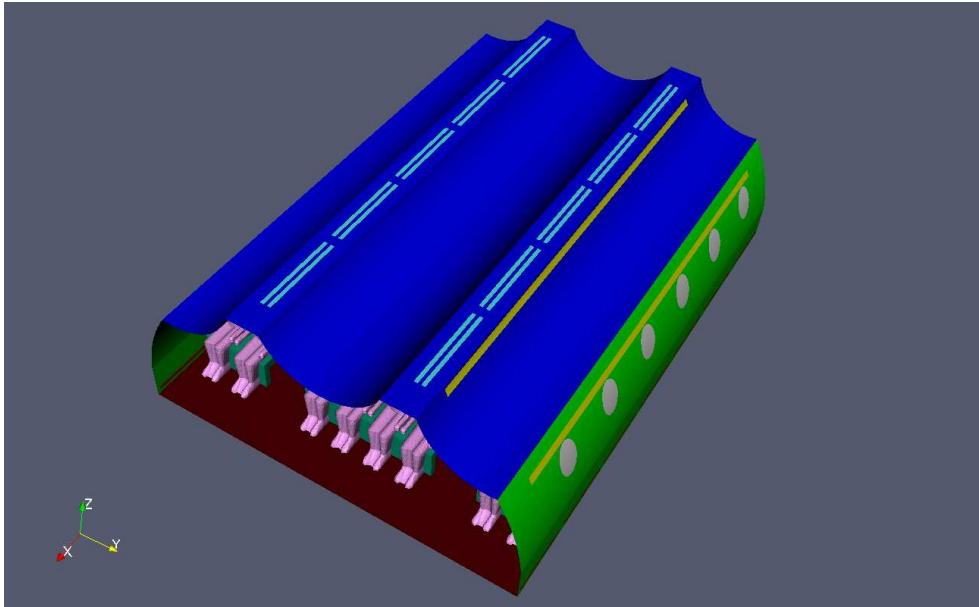
Figure 2. Generic wide-bodied aircraft cabin segment mock-up: air condition inlets (light blue) (top), air condition outlets (red), light-bands (yellow) and windows (gray) (bottom).

boundary part	color	condition		
dummies body	light pink	$q_\mathrm{w} = 68.55\frac{W}{m^2}$		$\varepsilon = 0.97$
dummies head, neck	yellow	$q_\mathrm{w} = 62.12\frac{W}{m^2}$		$\varepsilon = 0.97$
light-bands	light-yellow	$q_\mathrm{w} = 750.0\frac{W}{m^2}$		$\varepsilon = 0.97$
floor	dark-blue	$T_\mathrm{w} = 295.45K$	$\alpha_\mathrm{w} = 0.1645\frac{W}{m^2K}$	$\varepsilon = 0.8$
side-wall	light green	$T_\mathrm{w} = 295.45K$	$\alpha_\mathrm{w} = 0.2388\frac{W}{m^2K}$	$\varepsilon = 0.8$
cabin-windows	gray	$T_\mathrm{w} = 295.45K$	$\alpha_\mathrm{w} = 0.2388\frac{W}{m^2K}$	$\varepsilon = 0$
bottom	black	$T_\mathrm{w} = 295.45K$	$\alpha_\mathrm{w} = 0.2916\frac{W}{m^2K}$	$\varepsilon = 0.8$
front-wall	not visible	$T_\mathrm{w} = 295.45K$	$\alpha_\mathrm{w} = 7.1428\frac{W}{m^2K}$	$\varepsilon = 0.8$
back-wall	light-blue	$T_\mathrm{w} = 295.45K$	$\alpha_\mathrm{w} = 7.1174\frac{W}{m^2K}$	$\varepsilon = 0.8$
seat-tears	dark-green	adiabatic		$\varepsilon = 0.8$

Figure 3. Generic wide-bodied aircraft cabin segment mock-up: thermal boundary conditions (2) at the walls with fixed heat flux q_w or $q_\mathrm{w} = (T_\mathrm{w} - T)\,\alpha_\mathrm{w}$ with a fixed outer wall temperature T_w and the heat transfer coefficient α_w of the wall material and the emission coefficient ε. The colors are the marking colors of the different parts in figure 1.
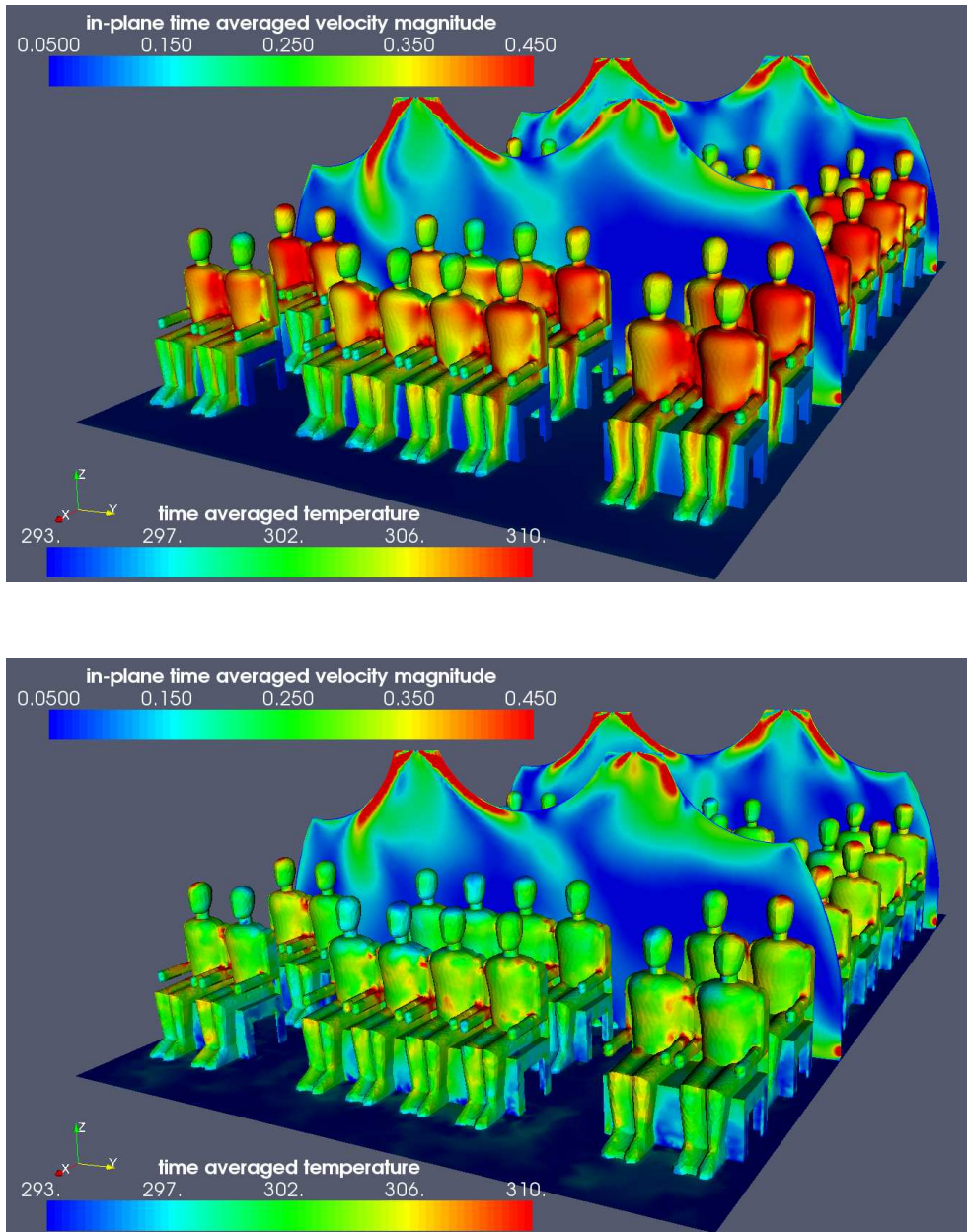
Figure 4. Generic wide-bodied aircraft cabin segment mock-up: Comparison of values without (top) and with (bottom) heat radiation. Here time averaged temperature distribution and in-plane time averaged velocity magnitude.
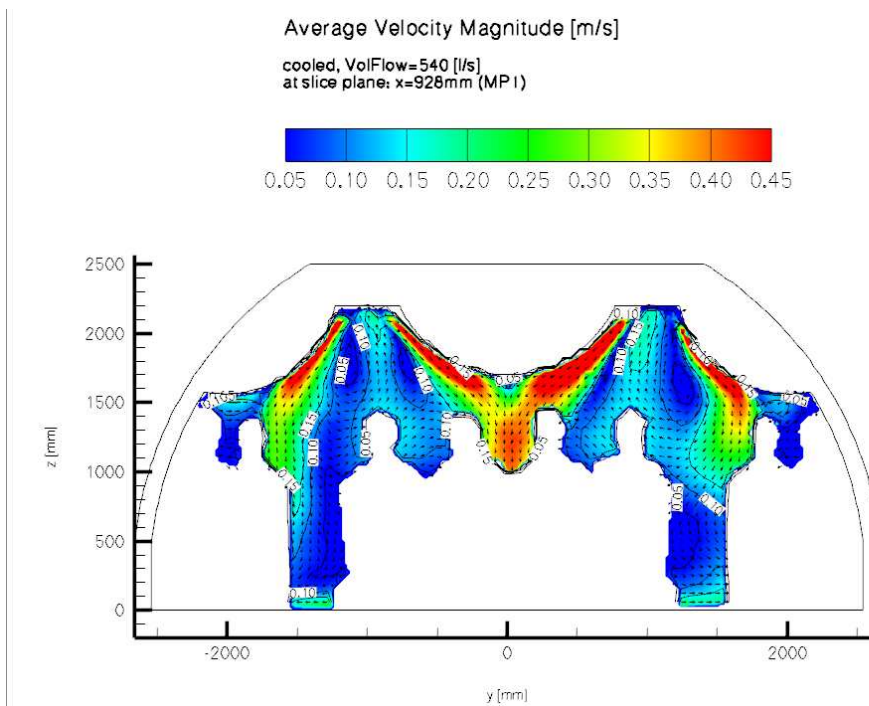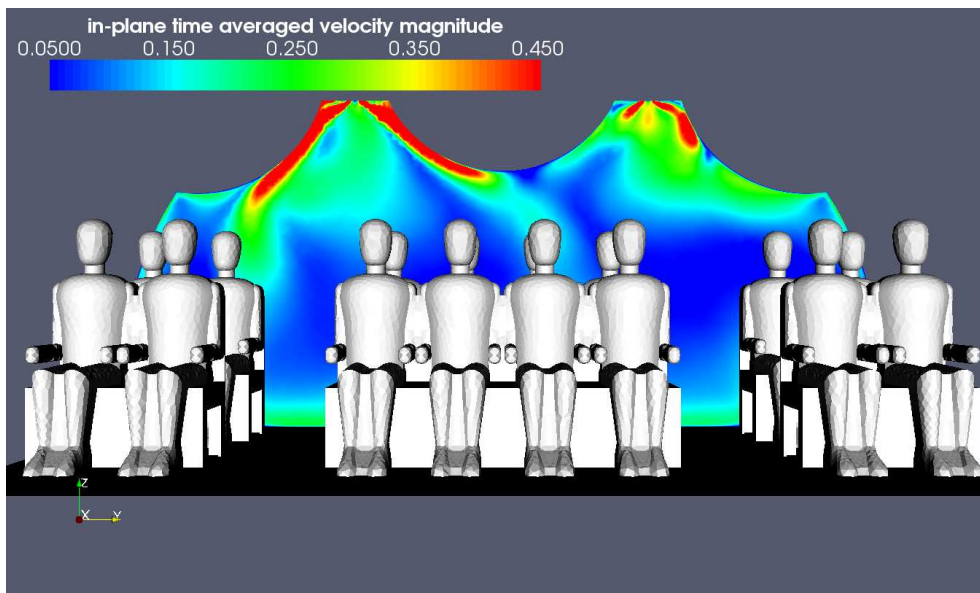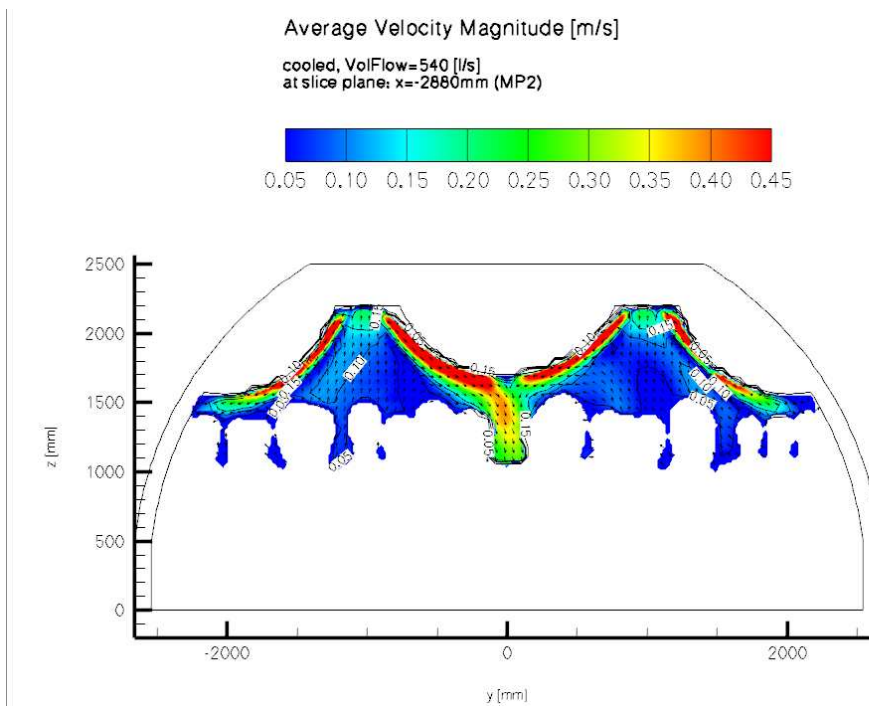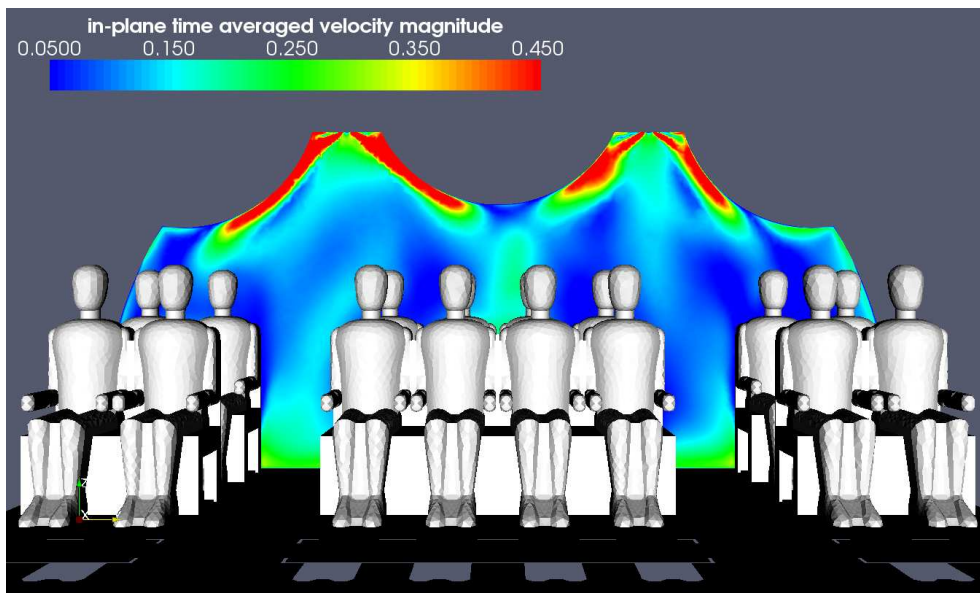
Figure 5. Generic wide-bodied aircraft cabin segment mock-up: Comparison of time averaged velocity magnitude obtained in the simulation (with radiation heat transfer) (top) and the PIV-data (bottom). Cut plane located in $x = 0.928m$.
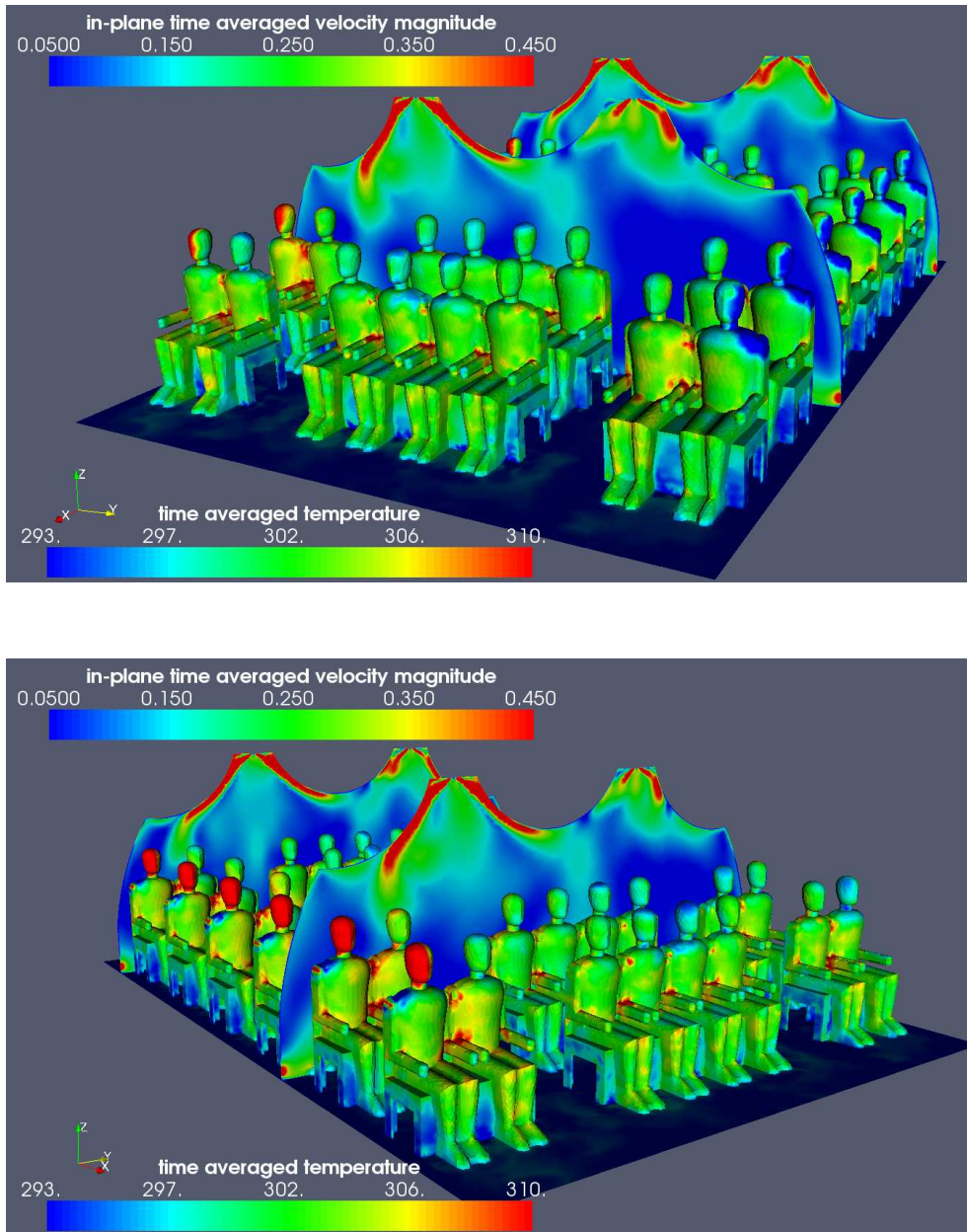
Figure 6. Generic wide-bodied aircraft cabin segment mock-up: Comparison of time averaged velocity magnitude obtained in the simulation (with radiation heat transfer) (top) and the PIV-data (bottom). Cut plane located in $x = -2.880$**.**

Figure 7. Generic wide-bodied aircraft cabin segment mock-up: View in the cabin from shadow side (top) and sun incidence side (bottom) respectively. Here time averaged temperature distribution and in-plane time averaged velocity magnitude.
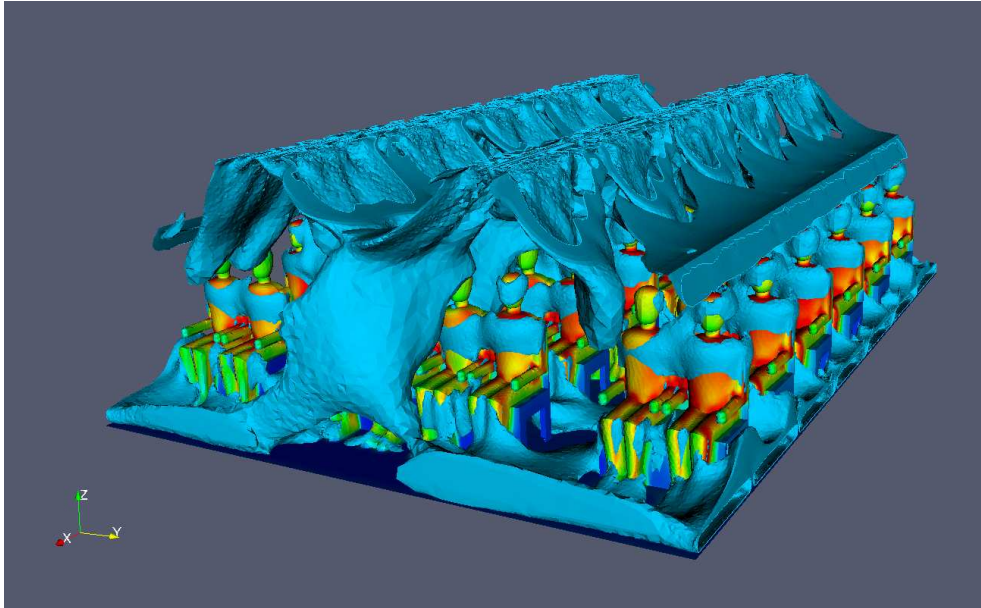
Figure 8. Generic wide-bodied aircraft cabin segment mock-up: Isoplanes of the time averaged velocity magnitude of value 0.2, no heat radiation.
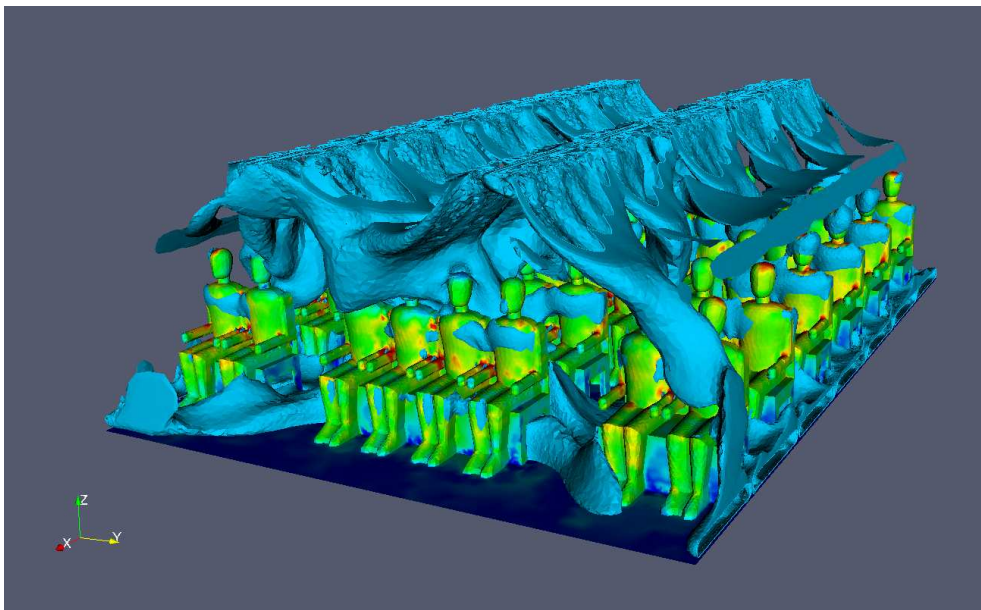

Figure 9. Generic wide-bodied aircraft cabin segment mock-up: Isoplanes for the time averaged velocity magnitude of value 0.2, heat radiation without sun incidence.
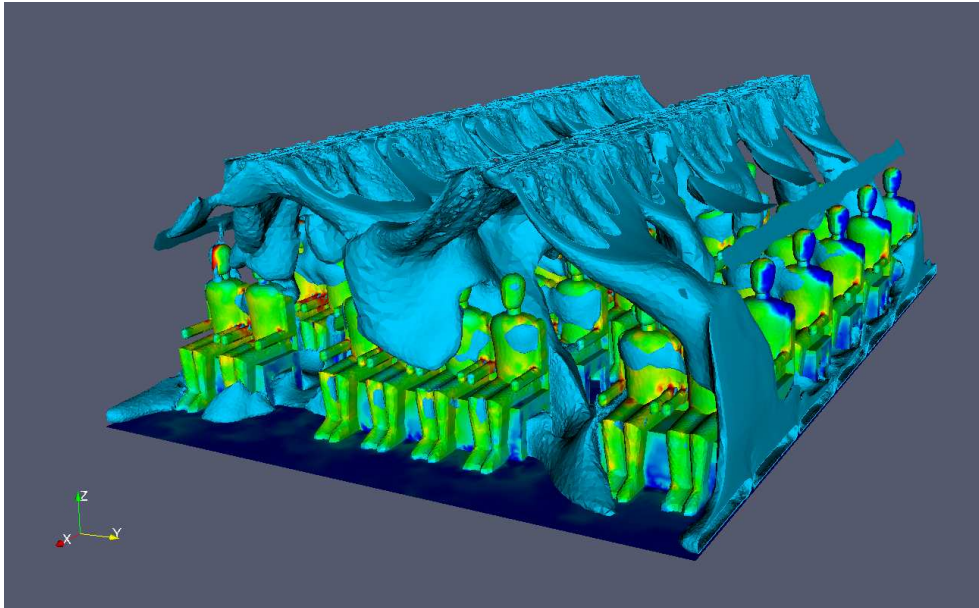
Figure 10. Generic wide-bodied aircraft cabin segment mock-up: Isoplanes for the time averaged velocity magnitude of value 0.2**, heat radiation with sun incidence.**
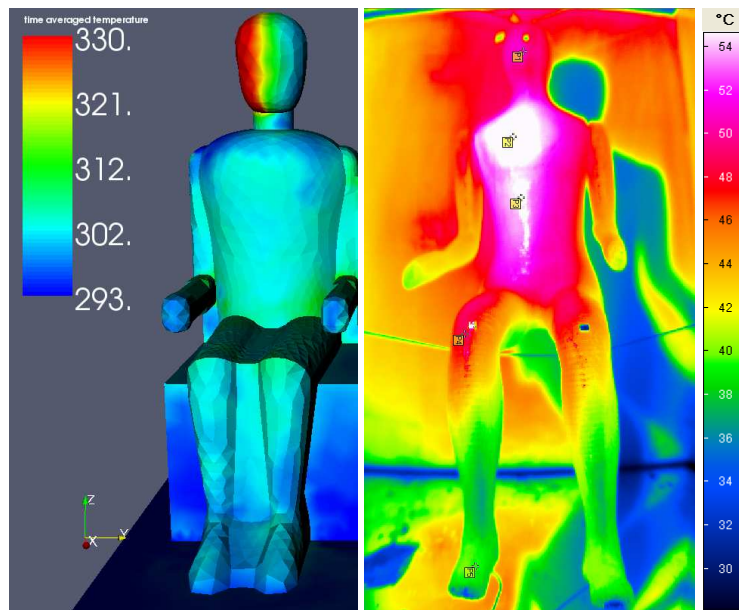

Figure 11. Time averaged surface temperature of the model dummy obtained in the simulation (left). Temperature distribution on the surface of a thermo model dummy which we used in the experiment set-up spotlighted from a distance of $1.89m$ **by a 1000 W lamp (right). The temperature at the marked points** $P1 : 50.79°C$**,** $P2 : 56.02°C$**,** $P3 : 55.60°C$**,** $P4 : 48.32°C$**,** $P5 : 39.54°C$**.**